Dalton Transactions

Accepted Manuscript

ROYAL SOCIETY OF CHEMISTRY

www.rsc.org/dalton

PEGylated FePt-Fe_3O_4 Composite Nanoassemblies (CNAs): *In vitro* Hyperthermia, Drug Delivery and generation of Reactive Oxygen Species (ROS)

Niroj Kumar Sahu,[1,2] Jagriti Gupta[1] and Dhirendra Bahadur[1*]

[1]*Department of Metallurgical Engineering and Materials Science, Indian Institute of Technology Bombay, Mumbai-400 076, India*

[2]*Centre for Nanotechnology Research, Vellore Institute of Technology University, Tamil Nadu-632014, India*

[*]Corresponding author: dhirenb@iitb.ac.in, Tel: +91-22-25767632, Fax: +91-22-2576 3480

Abstract

Chemothermal therapy is widely used in clinical application for treatment of tumor. But the major challenges are to use of multifunctional nano platform for significant regression of tumor. In this study, we report a facile synthesis of highly aqueous stable, carboxyl enriched, PEGylated mesoporous FePt/Fe_3O_4 composite nanoassemblies (CNAs) by a simple hydrothermal approach. CNAs exhibit high loading capacity ~90 wt. % of anticancer therapeutic drug, DOX due to its porous nature and availability of abundant negatively charged carboxylic groups on its surface. DOX loaded CNAs (DOX-CNAs) show pH responsive drug release in cell-mimicking environment. Further, the release is enhanced by application of AC magnetic field. CNAs show non-appreciable cytotoxicity in L929 but show toxic effects in cervical cancer (HeLa) cells at concentration of ~1mg/mL. A suitable composition of CNAs with a concentration of 2 mg/mL can generate hyperthermic temperature of ~ 43 ºC. Besides, CNAs, because of its Fe and Pt contents, has an ability to generate the reactive oxygen species (ROS) in presence of H_2O_2 inside the cancer cells which helps in enhancing its therapeutic effects. The synergistic combination of chemo and ROS is very efficient for killing of cancer cells.

1. Introduction

Cancer treatment through chemotherapy is a conventional practice since several decades. However, it has its own limitations like nonselective distribution of drugs, undesirable side effects on normal tissues and other physical inconveniences to the patients etc. Hence, there is a need to develop drug delivery (DD) systems in which specificity and localization can be tuned efficiently. In this regard, multifunctional nanoparticles (NPs) are practiced as an alternative carrier of therapeutics. This reduces the side effects of chemotherapy.[1,2] Magnetic NPs are frequently studied as a drug carrier because of their ability to be manipulated with an external magnetic field implying higher localization and heat generation in an alternating current magnetic field (ACMF) leading to hyperthermia treatment.[3,4] It is also reported that therapeutic efficacy of anticancer drug such as doxorubicin (DOX) is enhanced if combined with hyperthermia.[5,6] Among the magnetic NPs, Fe_3O_4 and FePt have emerged as better options due to their good biocompatibility, degradability under mild acidic conditions, catalytic and magnetic properties and capability to generate controlled noninvasive heat under an alternating current (AC) magnetic field (AMF).[3,4,7-11] Xu *et al.* has reported that FePt NPs release Fe in acidic pH solution which catalyzes H_2O_2 decomposition into reactive oxygen species (ROS) within cells that results in fast oxidation and deterioration of cellular membranes.[7] Recently Chen *et al.* discovered photothermal transduction efficiency of FePt NPs by the near infrared femtosecond laser irradiation which can be heated quickly to therapeutic temperature.[11] Fe_3O_4, on the other hand, exhibits higher heat dissipation capacity in ACMF and it shows a good catalytic behavior under specific conditions.[4,12] Hence, the combination FePt-Fe_3O_4 could be useful as a multifunctional platform for combination therapy.

Suitable surface functionalization of the NPs is an essential criterion for colloidal stability and biomedical applications. Several biocompatible dendritic and polymeric surface ligands like glycine based peptide mimic shell cross-linking,[4] alginate,[5] poly(N-isopropylacrylamide),[13] liposome,[14] etc. have been used to functionalize the magnetic NPs to enhance the properties and efficiency of the carrier. Further, for holding a large amount of drug at tumor site and to minimize the unwanted drug toxicity, mesoporous and hollow NPs have been used as they possess large specific surface area and pore volume.[3,15] Several reports discuss the synthesis of water dispersible mesoporous magnetic nanoassemblies, but those have their limitations due to toxicity and biodegradability concerns of ligands like polyacrylic acid,[16] and poly-glutamic acid.[15] When NPs or nanoassemblies are used for *in*

vivo applications, the common problems are the absorption of plasma proteins that leads to increase in size of the NPs, agglomeration, colloidal destabilization and non-specific uptake by reticular-endothelial system (RES), like macrophage cells. Also, these NPs are considered as intruder particles by the immunity system. This results in sequestering of the NPs from the blood circulation system and hence losing their function and efficiency. To overcome the above difficulties, proper surface functionalization of the NPs with hydrophilic and biocompatible polymer such as dextran,[17] dendrimers,[18] polyethylene glycol (PEG)[19] etc are usual practice. PEG is an amphiphilic polymer and is commonly regarded as a non-specifically interacting reducing reagent. Hence, it has been widely used for the conjugation with proteins to extend their circulation time.[20,21]

Based on the above observations, we prepared a novel, highly water dispersible, surface carboxyl enriched and mesoporous PEGylated FePt-Fe_3O_4 CNAs by a hydrothermal method. The resulting CNAs are demonstrated for use in drug delivery and *in vitro* chemo and thermal therapy for HeLa cancer cells (Scheme-1). Also, the generation of ROS by the catalytic response of CNAs has primarily been examined for future biomedical applications.

2. Experimental Details

2.1 Reagents and Materials

Analytical grade chemicals were used as received. Chloroplatinic acid hexahydrate ($H_2Pt(Cl)_6.6H_2O$, ≥37.5% Pt basis), Iron(II) chloride tetrahydrate ($FeCl_2.4H_2O$, >99%), Poly(ethylene glycol)bis(carboxy methyl)ether (HOOC-PEG-COOH, PEGD, M_w = 600) hydrazine hydrate solution (H_6N_2O,1L=1.03 Kg, 78-82%), Ethidium bromide ~95% (HPLC) and 2',7'-dichlorodihydrofluorescein diacetate (H_2DCFDA) were purchased from Sigma-Aldrich Co. (St. Louis, MO, USA). Dulbecco's modified eagle medium (DMEM), antibiotic-antimycotic solution (penicillin/streptomycin, P/S), Sulphorhodamine *B*(SRB), phosphate-buffered saline (PBS), Tris-buffered saline (TBS), trypsin-EDTA solution, trypan blue were obtained from Hi-Media Ltd (Mumbai, India). Acetic acid (glacial, 100%, Merck), paraformaldehyde (95%, Merck), trichloroacetic acid (TCA, 20% W/V, Loba Chemicals) and doxorubicin hydrochloride (DOX, ≥98%, Sigma Aldrich) were used in the experiment. L929 and HeLa cell lines were procured from the National Center of Cell Science (NCCS, Pune, India). MilliQ (18.2 MΩ-cm) water was used throughout the experiment.

2.2 Synthesis of PEGylated FePt-Fe_3O_4composite nanoassemblies (CNAs)

The CNAs was prepared using 4:1 molar ratio of Fe and Pt-precursors by hydrothermal method. In particular, 104 mg of $H_2PtCl_6.6H_2O$ and 160 mg of $FeCl_2.4H_2O$

were thoroughly dissolved in 15 mL of milli-Q water with magnetic stirring. 2 mL of hydrazine hydrate was added drop wise to the above solution which results in a change of the yellowish color solution to black. Then, 5 mL of PEGD was added and the solution was transferred to a specially designed teflon container (volume = 50 mL) and put in an air-tight steel based autoclave. It was heated in a box-furnace at 200 ºC for 24 h. Finally, the solution was cooled to room temperature and the material was washed five times in water-ethanol mixture followed by magnetic separation.

2.3 Characterization Techniques

The crystallographic identification and phase purity of the CNAs were analyzed by X-ray diffraction (XRD) using Philips powder diffractometer-PW3040/60. The average crystallite size was calculated using the Debye-Scherrer relation. Fourier transform infrared (FTIR) spectra of the dried powder samples were recorded in the range 400–4000 cm^{-1} using FTIR spectrometer (Magna550, Nicolet Instruments Co., USA). The particles distribution, morphologies and selected area electron diffraction (SAED) patterns of the CNAs were characterized by transmission electron microscopy (JEOL JEM-2100). Surface morphology has been identified by the Field Emission Scanning Electron Microscope (FEG-SEM, JEOL JEM-7600F). The compositional analyses were examined by energy dispersive X-ray spectroscopy (EDX) attached with FEG-SEM. Magnetic properties of the samples were measured in a physical properties measurement system (Quantum Design PPMS).The specific surface area, pore volume and pore size distributions of the CNAs were measured by Micromeritics instrument (ASAP 2020). The specific surface area is measured using multipoint Brunauer–Emmet–Teller (BET) method whereas; pore size distributions and total pore volume were determined by the Barrett-Joyner–Hallenda (BJH) method. Prior to measurements, the samples were outgassed at 90 ºC with a heating rate of 10 ºC/min for 1 h and then the temperature was raised up 140 ºC and maintained overnight. Zeta potentials of the colloidal particles were measured at different pH by zeta potential analyzer (Beckman Coulter Inc.). Hyperthermia studies were carried out in an Easy Heat 8310 (Ambrell, UK). For DOX loading and release experiment, fluorimeter (Varian Cary Eclipse) was used. Confocal laser scanning microscopy (CLSM) images were recorded on an Olympus inverted confocal microscope (ModelIX-81). The live/dead cells counting were performed in a hemocytometer.

2.4 DOX loading and release studies

The DOX loading capability of the CNAs was optimized by incubating 50 µg of DOX solution (conc. ~1 mg/mL) with different concentration of the materials. The total volume of the solution was made up to 1 mL by addition of DI water. The solutions in vials were incubated in a dark environment with constant shaking for 24 h. The loaded part was separated from the supernatant through centrifugation and the fluorescence spectra of the supernatant were recorded to calculate the entrapment efficacy. Finally, the optimized DOX loaded CNAs were used for *in vitro* study.

Drug release from optimized DOX loaded CNAs was performed at physiological pH (7.4) and mild acidic pH (4.3) environments with and without ACMF. DOX loaded CNAs were dispersed in 1 mL of buffer solution and transferred inside two separate membranes (Himedia, Dialysis membrane-150, LA401) with phosphate-buffered saline (PBS) of pH = 7.4 and sodium acetate buffer of pH = 4.3, respectively. The membranes with the loaded samples were kept separately in 20 mL PBS solution bath with constant stirring. The drug released from membranes into the PBS solution was collected at different time durations for analysis. The released DOX in the PBS was measured from fluorescence emission spectrum and percentage of release was estimated from fluorescence intensity. All the release experiments were performed in triplicate.

2.5 *In vitro* cell cytotoxicity studies

The cell culture experiments were carried out using L929 and HeLa cell lines. The cells were harvested in DMEM supplemented with 10% PBS and 1% P/S solution at 37 ºC in a saturated humidified environment of 5% CO_2 atmosphere (InCu-safe). *In vitro* cyto-compatibility of the CNAs was evaluated by SRB assay. The cells were seeded into 96-well plates (~1× 10^4 cells/well) and allowed to grow for 24 h. The loosely adhered cells were washed with PBS solution. The cells were then incubated with different concentrations of the CNAs. After 24 h, the plates were thoroughly washed with PBS and air-dried to remove excess water before processing for SRB assay. For cell fixation, 100 µL of ice-cold 10% TCA was added into each well at 4 °C for 1 h followed by washing with DI water. Then, 100 µL of 0.057% SRB was added and kept at room temperature for 20 min. Unbound SRB was washed away with 1% acetic acid (100 µL). To solubilize the dye, 100 µL of 10 mM TBS was added to each well and kept for 20 min. Thereafter, the plates were placed on a shaker to allow mixing and the absorbance (optical density, OD) was measured using a microplate spectrophotometer at 560 nm. The experiment was performed in triplicates. The percentage of viable cells was estimated using the formula:

$$\%\ \text{Cell viability} = \frac{\text{OD of treated cells}}{\text{OD of control cells}} \times 100$$

2.6 Cellular uptake of CNAs

Approximately 1×10^5 HeLa cells were seeded on glass cover-slip and placed in a 24-well culture plate and allowed to grow overnight as a monolayer. The surface adhered cells were then incubated with different concentration of CNAs taken from a stock media solution containing 2.0 mg per mL of CNAs or CNAs+DOX. After that, the cells were washed thoroughly with PBS and fixed with 300 µL of 10% paraformaldehyde. The excess paraformaldehyde was washed with PBS after 10 minutes. For confocal imaging the cover slips were placed on a glass slide and optical images of DOX were collected (λ_{ex} = 470 nm and λ_{em} = 590 nm).

2.7 *In vitro* study with CNAs in presence of H_2O_2 and determination ROS generation:

CNAs (50 and 25 µg mL^{-1}) along with 10 µg/mL of H_2O_2 were added to the medium cultured with cells at different pH (7.4 and 4.3). The cell viability was examined by SRB assay. For the determination of ROS, HeLa cells were seeded in 96-well plate at a concentration of ~1×10^4 cells/mL for 24 h followed by treatment with CNAs, Fe_3O_4 or FePt along with 10 µg/mL of H_2O_2. ROS is determined by adding H_2DCFDA to pretreated cultured cells and by recording the dichlorofluorescein (DCF) fluorescence at 535 nm. Determination of ROS was repeated 3 times independently. After the background subtraction, the fluorescence intensity of DCF is recorded by the plate reader. The ROS generation is expressed as ratio of fluorescence of DCF of treated cells to that of untreated cells.

2.8 *In Vitro* Hyperthermia study

The heating ability of dispersed CNAs was optimized by subjecting it to ACMF (frequency = 250 kHz and applied filed = 460 Oe) attached with a temperature monitoring probe. *In vitro* synergistic effect of DOX loaded CNAs (CNAs+DOX) on adherent HeLa cells was investigated in presence/absence of ACMF. The viability of treated cells was determined by the trypan blue method. Approximately, 1×10^6 cells were cultivated in a 30 mm petridish supplemented with 1 mL of DMEM. After 24 h, the cells were thoroughly washed with PBS and incubated with 1 mL CNAs+DOX (Conc.~ 2 mg mL^{-1}) and maintained at 37 ºC for 6 h along with negative and positive controls in triplicates. The petridishes containing cells were then exposed to ACMF (250 kHz, 460 Oe) for 25 minutes and the treated cells were kept inside the incubator for 24 h. After that, the petridishes were washed with PBS, trypsinized and collected via centrifugation for cell counting. The obtained cell

pellets after centrifugation at 2000 rpm were suspended in 900 µL of PBS and then 100 µL of 0.4% trypan blue was added to stain the dead cells. The percentage of viability was estimated by the formula:

$$\%\ \text{Viability} = \frac{\text{Live cells}}{\text{Total cells}} \times 100$$

3. Results and Discussion

3.1 Physical characterization

The XRD pattern of CNAs (Fig. 1) shows the diffraction lines of both the chemically disordered-FePt (cubic, JCPDS-29-0717) and magnetite Fe_3O_4 (inverse spinel, JCPDS-19-0696). This XRD pattern confirms the formation of FePt-Fe_3O_4 CNAs. Using Scherrer formula, the calculated crystallite sizes of FePt and Fe_3O_4 are ~ 9.4 and 10 nm, respectively. The lattice parameter of FePt and Fe_3O_4 are found to be 3.871 and 8.392Å, respectively. The volume fraction of Fe_3O_4 phase is less compared to that of FePt phase.

The surface chemical structure of the CNAs and PEGD has been characterized by FTIR spectroscopy and shown in Fig. S1. The characteristic bands at 1110 cm^{-1} (C–O–C stretch) and 1429 cm^{-1} (CH_2 scissor) have been observed in the CNAs. The characteristic bands of carboxylic group at 1666 cm^{-1} is found in CNAs that shifted by 90 cm^{-1} from the carboxyl band of HOOC-PEG-COOH indicating the binding of carboxylate groups to metal ions through the covalent interaction of one or two oxygen atoms with the metal.[3,22] A band at 1585 cm^{-1} could be attributed due to C-C stretching vibration in the CNAs. The bands at 2871 and 2943 cm^{-1} correspond to the symmetric and asymmetric stretching vibrations of the CH_2 group, respectively. The O-H stretching vibration of carboxyl group is observed at 3493 cm^{-1} which is at lower frequency than that of free O-H group indicating the presence of hydrogen bond. The Fe-O vibration at 575 cm^{-1} suggests the formation of magnetite phase.[23] The FTIR analysis confirms the coating of PEGD over the CNAs.

The microstructural and surface morphology of the CNAs are shown Fig. 2. Fig. 2a shows the SEM image of CNAs and the corresponding TEM micrograph is shown in Fig. 2b. SEM micrograph suggests near spherical shape for CNAs with mean diameter of ~ 65 nm. From the TEM micrograph, on the other hand it is seen that CNAs are well-defined, discrete and porous nanoassemblies in nature. Each nanoassembly is constituted by the several individual NPs of size about 8-9 nm which is in a good agreement with the crystallite size obtained from XRD line broadening. Surface area and porous nature of CNAs are also

investigated by using the nitrogen (N_2) adsorption–desorption isotherm plots and shown in Fig. S2. The isotherm profile indicates that the CNAs are mesoporous and possesses a specific surface area of 31 $m^2 \cdot g^{-1}$. The pore size distribution of average intra-pores and inter-pores diameters are ~3.5 and ~25 nm, respectively (inset of Fig. S2).

The STEM-EDX mapping has been performed to see the homogeneous distribution of Fe and Pt in CNAs. Fig. 3 shows the STEM-EDX spectra that confirms homogeneous distribution of Fe and Pt. It is not possible to distinguish between Fe_3O_4 and FePt phases due to the homogeneous distribution of both phases and lower volume fraction of magnetite phase. In this synthesis, N_2H_4 not only acts as a reducing agent but also helps in controlling the size to less than 100 nm. Simultaneously, PEG acts as a solvent, reducing and capping agent.[19] Apart from this, PEG serves as a cross linker between the NPs which might help in the formation of nanoassemblies. At the same time, individual magnetic NPs may also aggregate to form three-dimensional clusters by hydrogen bonding or anisotropic dipole–dipole or isotropic van der Waals coupling interactions.[24] The formation of the oxide phase (Fe_3O_4) along with FePt may be due to the absence of complete reducing atmosphere inside the autoclave. We believe that the FePt and Fe_3O_4 phases start nucleating at the beginning of reaction and by virtue of their very high surface energy; both these phases spontaneously attach and then aggregate to form three-dimensional clusters with assistance from PEG molecules. It is also possible that as the FePt phase starts nucleating during initial reaction, the surface of which gets partially oxidized to form Fe_3O_4. Therefore, these composite nanoparticles form right in the beginning of the reaction, which further aggregate to form clusters. To understand the formation of nanoassemblies, we have isolated the nanomaterials at different temperature condition of 120 ºC for 4h, 160 º for 4h, 200 ºC for 4h and 200ºC for 12 h. It is interesting to see that at low temperature of reaction itself (120 ºC for 4h), cluster formation starts to occur whereas, if there is an increase in temperature, more and more nanoparticles are assembled to form the larger clusters. When we keep the reaction for longer time at higher temperature (200 ºC for 12h), there is a further growth of the nanoclusters at the cost of individual nanoparticles as is demonstrated in Fig. S3. The HRTEM image in Fig S4a suggests that FePt (lattice spacing of ~2.2 Å corresponds to (111) plane) and Fe_3O_4 (lattice spacing of ~2.5 Å corresponds to (311) plane) are distributed throughout the nanoassembly. XRD and SAED patterns show that the CNAs are well crystalline in nature (Fig. 1 and Fig. S4b).

Functionalization of CNAs with PEG is also confirmed by the zeta potential measurement. Fig. S5 shows the variation in the zeta-potential of the suspension (0.2 mg/mL) at different pH values. Zeta potential of CNAs suggests the functionalization of CNAs with the PEG. Zeta potential of CNAs shows negative potential at high pH probably due to the presence of negatively charged carboxylate ions on the surface of the CNAs. The carboxyl enriched PEGylated CNAs gives good stability in aqueous suspension. (The pH of zero point charge (pH_{pzc}) is found to be around 3.5. Thus, the CNAs have net positive surface charge at pH < pH_{pzc} and negative surface charge at pH >pH_{pzc}. The positive charge on the surface below pH_{pzc} is due to availability of excess H^+ ions (positively charged) which passivate the carboxyl enriched (COO^-, negatively charged) surface of CNAs by electrostatically neutralizing it). Negative zeta potential of CNAs makes this carrier suitable for the positively charged DOX. This may be attributed primarily to the electrostatic interactions between positively charged DOX molecules and negatively charged carboxyl moieties present on the surface of CNAs. Furthermore, the mesoporous nature, size of CNAs below 100 nm, abundant surface carboxylation and high specific surface area make these assemblies an ideal nanocarrier for drug delivery applications.

Fig. S6 shows the room temperature field dependent magnetization (M *vs.* H) plots of CNAs. The M–H plot shows a typical superparamagnetic nature of the CNAs with magnetization of 50.7 emu g^{-1}. Inset of Fig. S6 (top left corner) shows the ZFC-FC plot of the CNAs. Form the ZFC-FC plots, a blocking temperature (T_B) of CNAs is observed at ~250 K. Additionally, another transition is observed in ZFC plot at temperature of ~130 K which is typical of verway transition. This transition is due to the presence of Fe_3O_4 in CNAs.[25] Insets of the Fig S6 (bottom right corner) show the colloidal suspension of the CNAs and its tendency to get attracted towards the bar magnet. Fig. S7 shows the temperature *vs.* time plots of CNAs under AC magnetic field (ACMF). During the same time, the heating ability of Fe_3O_4 nanoassemblies (2 mg/mL) and only water was measured as control. The results show a time dependent gradual increase in temperature. It has been observed that the dispersion of CNAs (Conc. ~ 2 mg/mL) with the application ACMF (frequency ~ 250 KHz, field strength ~ 460 Oe), is able to generate the hyperthermia temperature of ~43 ºC in 15 minutes. There is essentially no generation of heat in only water. However, a steep rise in temperature is observed in Fe_3O_4 nanoassemblies and ~43 ºC is achieved in ~5 minutes at the same frequency and field.

3.2 Biological characterization

To examine the feasibility of this nanoassembly in bio-related fields, the cytotoxicity was investigated using L929 and HeLa cells by SRB assay. Fig. S8 shows the effect of CNAs on the cell proliferation on both L929 and HeLa cells. The results show that CNAs do not have any effect on the cell proliferation of L929. Therefore, this material is quite biocompatible for L929 cells on treatment with the concentration of CNAs up to 2.0 mg mL^{-1} for 24 h incubation. These results indicate that the CNAs have low cytotoxicity towards normal mouse fibroblast cell line (L929 cells).[26] However, the CNAs show some toxic effect towards HeLa cancer cells. More than 20% of cells died at the same concentration after 24 h incubation. Xu *et al.* reported that FePt NPs release Fe under mild acidic condition (pH ~4.3) while it is chemically inert in neutral pH (7.4). The released Fe catalyzes H_2O_2 decomposition in intracellular environments by Fenton's reaction and generates the reactive oxygen species (ROS). These are highly reactive for lipid membrane oxidation and inhibit tumor growth.[7] Therefore; we have further investigated the role of CNAs towards the generation of the reactive oxygen species (ROS).

3.3 *In vitro* drug loading, release and investigation of ROS generation

Fig. 4 shows the fluorescence spectra of DOX with CNAs. This has been used to investigate the interactions of drug molecules with CNAs and to estimate the loading efficiency. The entrapment efficiency of drug in CNAs has been monitored with fluorescence intensity of DOX (supernatant) separated from loaded sample. From the fluorescence spectra, it is observed that the florescence intensity of DOX is not affected by the change in pH of the solution. Hence, the mechanism of loading and release depends on the functionalization of the NPs and the chemical attachment of DOX over it.[27] High entrapment efficiency of ~79% is observed when 50 µg of DOX is incubated with 10 mg of CNAs in 1 mL of water. This is due to the mesoporous nature, significant specific surface area and abundance of carboxyl groups ($-COO^-$) on the surface of CNAs which bind electrostatically with amine groups of DOX. The polymeric nature of PEG-diacid also plays an additional role for higher entrapment. This has been clearly indicated in the decrease profile of fluorescence intensity of DOX (unloaded part) after loading with the above materials.

Fig. 5 shows the cumulative DOX release profiles from DOX loaded CNAs over a period at different pH of 4.3 and 7.4 with and without ACMF. The drug release studies were performed under reservoir-sink conditions (reservoir: pH 4.3/pH 7.3 and sink: pH 7.3). This mimics the endosomal environment of cancer cells and physiological one. The release rate of DOX from loaded CNAs is higher in the acidic endosomal environment. The overall release

of DOX from CNAs in both environments show essentially sustained release pattern. DOX release is stimulus to pH and thus can occur across the range of pH values found in intracellular lysosomes of cancerous tissues and its local environment (pH~4 or 5). This suggests that targeted therapeutic capacity can be enhanced by passive release at the pathologically relevant sites. The drug release profiles have two distinct linear rates. The initial stage of burst release up to 10 h, during which 11.5 ± 2.9 % and 45.2 ± 2.3 % of DOX were released from the CNAs at pH 7.4 and 4.3, respectively which can be attributed to the release of surface adsorbed drug molecules.[28] Moreover, the faster diffusion rate at initial stage may be due to the higher concentration gradient of drug from matrix to the release medium which slows down steadily with passage of time as the equilibrium is attained. This is in accordance with Higuchi drug release model confirming that the DOX release process is diffusion-controlled.[4] It is seen that if bare DOX solution is kept in the membrane and the drug release is performed in the above stated reservoir-sink conditions, the burst release of DOX occurs irrespective of different pH.[27] This indicates that the mechanism of DOX attachment and its release are dependent on the materials behavior and its surface functionality. The overall release efficiency is higher at lower pH (4.3) than at physiological pH (7.4) which is important for the killing of relatively acidic tumor cells. The higher cumulative drug release efficiency in the acidic conditions might be due to the presence of -COO^- group on the surface of CNAs which has the higher affinity towards abundant H^+ than -NH_3^+. The COO^- group could be partially neutralized by H^+ ions and eventually the electrostatic interaction between the DOX and -COO^- on the surface of CNAs is weak. Alternatively, as the pKa value of carboxylate group is about ~ 4.8 and hence carboxylate group may be dissociated in the solution (~ pH = 4.3). Also, if pH is decreased, increase protonation of $–NH_2$ groups on DOX may lead to enhanced drug release. Overall, the release is favored in acidic condition. These comparative results reveal the pH sensitivity of drug release. Also, such observations have been reported in many different systems.[3,29,30] DOX release experiments were also performed in the presence of AC magnetic field. It has been seen that DOX release is significantly enhanced with the application of field. This behavior is observed in both the pH (4.3 and 7.4) conditions. This may be due to the interaction of magnetic CNAs with the oscillating alternating magnetic field resulting in the enhancement of Brownian motion of particles. Because of the increase in Brownian motion, there may be mechanical force which works as a stimuli and favors the release of DOX. Interestingly, there is more than 90% cumulative drug release with the application of ACMF in less than 60

minutes which will be beneficial in targeted tumor treatment. The applied ACMF helps in diffusion of drugs through bond breaking by the strong mechanical force generated by the magnetic particles under AC field implying enhanced drug release.[14]

Decomposition of H_2O_2 which is catalyzed by Fe, generates reactive oxygen species such as the hydroxyl radical (OH•). These ROS oxidizes various organic molecules including membrane lipids, DNA, and proteins in cells. Therefore, Fe in cellular systems can produce ROS which induce oxidative stress leading to cellular damage and cell death.[31] Sun *et al.* proposes a better control in Fe buildup process for cancer therapy using FePt NPs as a Fe reservoir.[7] In this context, we have investigated the ROS generation using CNAs and compared the results with that of Fe_3O_4 and Pt. It has been observed that CNAs exhibit higher efficiency of generation of ROS as compared to Fe_3O_4 and Pt which will assist in treatment of cancerous cells. Fig. 6 shows the generation of ROS in HeLa cells. It may be mentioned that Fe_3O_4 and Pt nanoassemblies were prepared adopting the same method of preparation of CNAs. The significant change of ROS for CNAs might be due to the synergistic catalytic effect of both FePt and Fe_3O_4 in the assemblies.

3.4 *In vitro* cytotoxicity study for HeLa cells

The cytotoxicity effect on HeLa cell lines due to DOX release from DOX loaded CNAs was investigated. Fig. S9 shows the cytotoxicity of CNAs+DOX along with CNAs as control. From the cytotoxicity study, it has been observed that bare CNAs show some effect on the cell proliferation of HeLa cell after 24 h treatment, whereas a clear cytotoxic effect could be observed in the case of CNAs+DOX due to the release of DOX in the cells. The cytotoxic effect sequentially increased with the increase in the concentration. ~70 % of HeLa cells had undergone apoptosis at a concentration of 2.0 mg/mL of CNAs+DOX (DOX content ~9 μg). The higher concentration results eventually in more release of DOX inside the cells inducing cell death.

To enhance the chemotherapic effect of CNAs+DOX, magnetic hyperthermia has been employed to investigate the synergistic effect on cancer therapy. Fig. 7 shows the viability of HeLa cells incubated with CNAs+DOX in presence and absence of AC magnetic field. It has been observed that the control cells without ACMF do not show much decrease in cell viability. On the other hand if the HeLa cells are exposed to ACMF on treatment with 2 mg of CNAs, only ~ 53 ± 2.1% the cells are alive. The ACMF has been applied for a total of 25 min, 15 min for reaching the hyperthermic temperature and 10 more minutes to expose at this temperature. Similarly, ~ 48 ±4.7 % cells are live when the cells are treated with DOX.

However, less than 20% is seen live on treatment with CNAs + DOX with the applied ACMF. This may be due to the synergistic effect of both chemo and thermotherapy. It is also evidenced from Fig. 5 that the DOX release from CNAs is more at lower pH and it gets further enhanced with the application of ACMF and hence a collective impact is observed. The morphological changes of HeLa cells are clearly seen in the optical images and shown in the Fig. 8. The density of live cells is observed to decrease considerably in treated cells as compared to control one (Fig. 8 a and b). It is observed that on treatment with bare DOX, the morphology changes significantly to rounded shape and catastrophic cell death is observed (Fig. 8b). However, there is a controlled way of killing the cells with CNAs + DOX as there is sustained release of DOX (Fig. 8c). When cells were treated with CNAs+DOX in ACMF, the apoptosis of cancer cells is observed through cell membrane blebbing and shrinkage in cell volume due to chemo-thermal therapy (Fig. 8d). The external heat generates mechanical stress on the cell wall leading to shrinkage. Yoo *et al.*[32] demonstrated that cancer cell's death by hyperthermia treatment is caused through apoptosis rather than the necrosis which implies that the present composite nanoassemblies system would be a potential agent for thermal therapy of cancer. Further, the morphological assessment has been done through CLSM for the cells when treated with DOX loaded CNAs. Fig. 9 shows the fluorescence image of HeLa cells stained with ethidium bromide (nucleus staining dye). Fig. 9 (a and b) shows the fluorescence image of HeLa cells treated with DOX for 4 and 24 h. It is clearly observed that there is catastrophic cell death with bare DOX (Conc. ~ 9 μg/mL) as the time of treatment increases from 4 to 24 h. The cell membrane shrinks significantly. Fig. 9 (c and d) shows the fluorescence image of HeLa cells treated DOX loaded CNAs. However, in Fig. 9 (c and d), apoptosis occurs in a control way through cell membrane blebbing and denaturation of nuclear compartment on CNAs + DOX. After 4h of treatment, cell morphology does not change much whereas after 24 h of treatment, a significant change in the cell membrane, complete DNA fragmentation and a reduction in size of the nucleus of HeLa cells is observed. This indicates that apoptosis process occurs on treatment with the DOX loaded CNAs.

3.5 *In vitro* cytotoxicity study for HeLa cells through ROS generation

It is well known that Pt NPs show good catalytic behavior.[33] Also, it has been reported that platinum in the alloy form *e.g.* FePt shows enhanced catalytic activity because of the availability of more number of reactive/active sites.[34] Recently Fe_3O_4 has also been used for generation of ROS for cancer treatment.[35] Fig. 10 shows the *in vitro* treatment of HeLa cells

with CNAs and CNAs+DOX at different pH conditions in presence of 10 µg/mL of H_2O_2. H_2O_2 itself does not show any toxic effect to cells at pH 7.4 and 4.3. However, when cells are treated with 10 µL of H_2O_2 along with 25 µL CNAs, viability of ~41.2±4.5 and ~33.9±3.9 % are achieved at pH 7.4 and 4.3, respectively. From ICP-AES results (Fig. S10), it is observed that CNAs get slowly dissolved in the acidic environment (pH~4.3) and Fe ions are released which is supposed to catalyze the H_2O_2 by Fenton's reaction.[7] The Fenton's reaction suggests that hydrogen peroxide is dissociated by Fe^{2+} or Fe^{3+} ions through the process of oxidation or reduction of Fe ions forming a hydroxyl radical or hydroperoxyl radical as follows:

(1) $Fe^{2+} + H_2O_2 \rightarrow Fe^{3+} + HO\bullet + OH^-$ or

(2) $Fe^{3+} + H_2O_2 \rightarrow Fe^{2+} + HOO\bullet + H^+$

Further toxicity effect is observed when 50 µL of CNAs and CNAs+ DOX was added to 10 µg/mL of H_2O_2. This happens because of the generation of ROS which provides oxidative stress on the cell membrane resulting in cell death. Interestingly, almost complete cell death is observed when 10 µL of H_2O_2 is incubated along with CNAs+DOX in acidic pH condition. This may be due to the synergistic effect of release of DOX as well as the enhanced ROS generation. Hence, this system could serve as a potential probe for cancer therapy.

4. Conclusion

Multifunctional composite nanoassembly of Fe_3O_4 and FePt was synthesized by hydrothermal method and used as a potential carrier of anticancer therapeutic. The CNAs show the potential for carrying the DOX with high entrapment efficiency and the release behavior is pH stimulated. Better killing is observed for HeLa cells when treated with DOX loaded CNAs in hyperthermic condition due to the combined effect of chemo and thermo therapy. However, almost complete cell death is observed when the cells are treated with DOX loaded CNAs in the presence of H_2O_2 in acidic pH. This is because of the synergistic effect of ROS and chemotherapy. These unique combinations of chemotherapy, thermotherapy and ROS generation could be one of the most effective ways for the treatment of tumor in this surface engineered composite nanoassembly system.

Supplementary materials:

† Electronic supplementary information (ESI) available: FTIR, HRTEM, Zeta potential, M-H plot, Hyperthermia, Porosity, cell biocompatibility study etc. are described.

Acknowledgement

Authors are thankful to Nanomission of Department of Science and Technology (DST) and nanotechnology division of Department of Electronics and Information Technology (DEITY), Government of India for financial support. The TEM and SEM facilities provided by the CRNTS, IIT Bombay are acknowledged.

Figure Caption

Fig. 1 XRD pattern of CNAs. The symbols # and * indicate the FePt and Fe_3O_4 phase, respectively.

Fig. 2 (a) FESEM and (b) TEM image of the CNAs.

Fig. 3 (a) STEM image of the CNAs, Fig.3 (b and c) EDX spectra (area scanned) showing the variation of Fe and Pt and Fig.3 (d and e) line scanned images.

Fig. 4 Fluorescence spectra of the supernatant (unloaded part) after loading of 50 μg of DOX with different concentration of CNAs. The incubation time was kept fixed for 24 h. The excitation wavelength is 470 nm and the emission range is scanned between 490 and 700 nm.

Fig. 5 Cumulative drug release profile from DOX loaded CNAs in cell mimicking environment at pH 7.4 and 4.3 without (a) and with (b) application of ACMF. PBS solution was taken as reservoir.

Fig. 6 Percentage change of ROS over control after treatment with different concentration of CNAs.

Fig. 7 *In vitro* cytotoxicity of HeLa cell lines with DOX, CNAs and CNAs + DOX with or without ACMF.

Fig. 8 Microscopic images of HeLa cells: (a) control, (b) after treatment with bare DOX, (c) after treatment with DOX loaded CNAs and (d) after treatment with DOX loaded CNAs in hyperthermia condition. All scale bars are 200 μm.

Fig. 9 Confocal laser scanning microscopy (CLSM) images show the apoptosis (DNA fragmentation) in HeLa cells. (a and b) with DOX (9 μg/mL) at indicated time intervals of 4 and 24 h, (c and d) with DOX loaded CNAs at indicated time intervals of 4 and 24 h. The green fluorescence shows the presence of DOX in DOX loaded CNAs, red fluorescence shows ethidium bromide (EtBr) stained nuclei. The scale bar is 50 μm.

Fig. 10 *In vitro* cytotoxicity of HeLa cell lines with H_2O_2, CNAs+H_2O_2 and CNAs+DOX+H_2O_2 along with the control. The volume taken for H_2O_2 was 10 μL.

References

(1) R. A. Petros and J. M. DeSimone, Strategies in the design of nanoparticles for therapeutic applications. *Nat. Rev. Drug Disc.* 2010, **9**, 615-627.

(2) S. Chandra, K. C. Barick and D. Bahadur, Oxide and hybrid nanostructures for therapeutic applications. *Adv. Drug Del. Rev.* 2011, **63**, 1267-1281.

(3) S. Kumar, A. Daverey, N. K. Sahu and D. Bahadur, In vitro evaluation of PEGylated mesoporous $MgFe_2O_4$ magnetic nanoassemblies (MMNs) for chemo-thermal therapy. *J. Mater. Chem. B* 2013, **1**, 3652-3660.

(4) K. C. Barick, S. Singh, ,N. V. Jadhav, D. Bahadur, B. N. Pandey and P. A. Hassan, pH-Responsive Peptide Mimic Shell Cross-Linked Magnetic Nanocarriers for Combination Therapy, *Adv. Funct. Mater.* 2012, **22**, 4975-4984.

(5) S. Brule, M. Levy, C. Wilhelm, D. Letourneur, F. Gazeau, C. Menager and C. Le Visage, Doxorubicin Release Triggered by Alginate Embedded Magnetic Nanoheaters: A Combined Therapy, *Adv. Mater.* **2011,** *23*, 787-790.

(6) C. R. Thomas, D. P. Ferris, J. H. Lee, E. Choi, M. H. Cho, E. S. Kim, J. F. Stoddart, J. S. Shin, J. Cheon and J. I. Zink, Noninvasive Remote-Controlled Release of Drug Molecules in Vitro Using Magnetic Actuation of Mechanized Nanoparticles, *J. Am. Chem. Soc.* 2010, **132**, 10623-10625.

(7) C. J. Xu, Z. L. Yuan, N. Kohler, J. M. Kim, M. A. Chung and S. H. Sun, FePt Nanoparticles as an Fe Reservoir for Controlled Fe Release and Tumor Inhibition, *J. Am. Chem. Soc.* 2009, **131**, 15346-15351.

(8) T. Fuchigami, R. Kawamura, Y. Kitamoto, M. Nakagawa and Y. Namiki, A magnetically guided anti-cancer drug delivery system using porous FePt capsules, *Biomaterials* 2012, **33**, 1682-1687.

(9) N. K. Sahu and D. Bahadur, Influence of excess Fe accumulation over the surface of FePt nanoparticles: Structural and magnetic properties, *J. Appl. Phys.* 2013, **113**, 134303-134312.

(10) N. K. Sahu, A. Prakash, and D. Bahadur, Role of different platinum precursors on formation and reaction mechanism of FePt nanoparticles and their electrocatalytic performance towards methanol oxidation, *Dalton Trans.* 2014, **43**, 4892-4900.

(11) C. L. Chen, L. R. Kuo, S. Y. Lee, Y. K. Hwu, S. W. Chou, C. C. Chen, F. H. Chang, K. H. Lin, D. H. Tsai and Y. Y. Chen, Photothermal cancer therapy via femtosecond-laser-excited FePt nanoparticles, *Biomaterials* 2013, **34**, 1128-1134.

(12) D. Zhang, Y. X. Zhao, Y. J. Gao, F. P. Gao, Y. S. Fan, X. J. Li, Z. Y. Duan, H. Wang, Anti-bacterial and in vivo tumor treatment by reactive oxygen species generated by magnetic nanoparticles, *J. Mater. Chem. B* 2013, **1**, 5100-5107.

(13) M. K. Jaiswal, M. Gogoi, H. D. Sarma, R. Banerjeeb and D. Bahadur, Biocompatibility, biodistribution and efficacy of magnetic nanohydrogels in inhibiting growth of tumors in experimental mice models, *Biomater. Sci.*, 2014, **2**, 370-380.

(14) L. Pradhan, R. Srivastava and D. Bahadur, pH- and thermosensitive thin lipid layer coated mesoporous magnetic nanoassemblies as a dual drug delivery system towards thermochemotherapy of cancer, *Acta biomaterialia,* 2014, **10**, 2976-2987.

(15) Luo, B.; Xu, S. A.; Luo, A.; Wang, W. R.; Wang, S. L.; Guo, J.; Lin, Y.; Zhao, D. Y.; Wang, C. C., Mesoporous Biocompatible and Acid-Degradable Magnetic Colloidal Nanocrystal Clusters with Sustainable Stability and High Hydrophobic Drug Loading Capacity, *Acs Nano* 2011, **5**, 1428-1435.

(16) J. P. Ge, Y. X. Hu, M. Biasini, W. P. Beyermann and Y. D. Yin, Superparamagnetic magnetite colloidal nanocrystal clusters, *Angew. Chem.* 2007, **46**, 4342-4345.

(17) C. Tassa, S. Y. Shaw and R. Weissleder, Dextran-Coated Iron Oxide Nanoparticles: A Versatile Platform for Targeted Molecular Imaging, Molecular Diagnostics, and Therapy, *Acc. Chem. Res.* 2011, **44**, 842-852.

(18) B. Pan, D. Cui, Y. Sheng, C. Ozkan, F. Gao, R. He, Q. Li, P. Xu and T. Huang, Dendrimer-modified magnetic nanoparticles enhance efficiency of gene delivery system. *Cancer Res.* 2007, **67** , 8156-8163.

(19) C. Sun, K. Du, C. Fang, N. Bhattarai, O. Veiseh, F. Kievit, Z. Stephen, D. Lee, R. G. Ellenbogen, B. Ratner and M. Zhang, PEG-mediated synthesis of highly dispersive multifunctional superparamagnetic nanoparticles: their physicochemical properties and function in vivo, *ACS Nano* 2010, **4**, 2402-2410.

(20) S. M. Moghimi, A. C. Hunter and J. C. Murray, Long-circulating and target-specific nanoparticles: Theory to practice, *Pharmacological Rev.* 2001, **53**, 283-318.

(21) V. P. Torchilin and V. S. Trubetskoy, Which polymers can make nanoparticulate drug carriers long-circulating? *Adv. Drug Del. Rev.* 1995, **16**, 141-155.

(22) F. Q. Hu, K. W. MacRenaris, E. A. Waters, E. A. Schultz-Sikma, A. L. Eckermann and T. J. Meade, Highly dispersible, superparamagnetic magnetite nanoflowers for magnetic resonance imaging, *Chem. Comm.* 2010, **46**, 73-75.

(23) X. H. Sun, C. M. Zheng, F. X. Zhang, Y. L. Yang, G. J. Wu, A. M. Yu and N. J. Guan, Size-Controlled Synthesis of Magnetite (Fe_3O_4) Nanoparticles Coated with Glucose and Gluconic Acid from a Single Fe(III) Precursor by a Sucrose Bifunctional Hydrothermal Method. *J. Phys. Chem. C* 2009, **113**, 16002-16008.

(24) A. Baskin, W. Y. Lo and P. Kral, Clusters and lattices of particles stabilized by dipolar coupling, *ACS Nano* 2012, **6**, 6083-6090.

(25) T. J. Daou, G. Pourroy, J. M. Greneche, A. Bertin, D. Felder-Flesch, S. Begin-Colin, Water soluble dendronized iron oxide nanoparticles, *Dalton trans.* 2009, 4442-4449.

(26) M. Babincova, P. Sourivong, D. Leszczynska and P. Babinec, Blood-specific whole-body electromagnetic hyperthermia, *Med. Hypotheses* 2000, **55**, 459-60.

(27) N. K. Sahu, N. S. Singh, L. Pradhan and D. Bahadur, Ce^{3+} sensitized $GdPO_4$:Tb^{3+} with iron oxide nanoparticles: a potential biphasic system for cancer theranostics. *Dalton Trans.* 2014, **43**, 11728-11738.

(28) Y. Mi, X. L. Liu, J. Zhao, J. Ding and S. S Feng, Multimodality treatment of cancer with herceptin conjugated, thermomagnetic iron oxides and docetaxel loaded nanoparticles of biodegradable polymers, *Biomaterials* 2012, **33**, 7519-7529.

(29) W. Chen, F. Meng, R. Cheng and Z. Zhong, pH-Sensitive degradable polymersomes for triggered release of anticancer drugs: a comparative study with micelles, *J. Control Release* 2010, **142**, 40-46.

(30) F. Zhang, G. B. Braun, A. Pallaoro,Y. C. Zhang, Y. F. Shi, D. X. Cui, M. Moskovits, D. Y. Zhao and G. D. Stucky, Mesoporous Multifunctional Upconversion Luminescent and Magnetic "Nanorattle" Materials for Targeted Chemotherapy, *Nano Letters* 2012, **12**, 61-67.

(31) G. Papanikolaou and K. Pantopoulos, Iron metabolism and toxicity, *Toxicol. Appl. Pharmacol.* 2005, **202**, 199-211.

(32) D. Yoo, J.-H. Lee, T.-H. Shin and J. Cheon, Theranostic Magnetic Nanoparticles. *Acc. Chem. Res.* 2011, **44**, 863-874.

(33) J. H. Gao, H. W. Gu and Xu, B., Multifunctional Magnetic Nanoparticles: Design, Synthesis, and Biomedical Applications, *Acc. Chem. Res.* 2009, **42**, 1097-1107.

(34) W. Li, W. Zhou, H. Li, Z. Zhou, B. Zhou, G. Sun and Q. Xin, Nano-stuctured Pt–Fe/C as cathode catalyst in direct methanol fuel cell. *Electrochimica Acta* 2004, **49**, 1045-1055.

(35) D. Zhang, Y.-X. Zhao, Y.-J. Gao, F.-P. Gao, Y.-S. Fan, X.-J. Li, Z.-Y. Duan, and H. Wang, Anti-bacterial and in vivo tumor treatment by reactive oxygen species generated by magnetic nanoparticles, *J. Mater. Chem. B* **2013,** 1, 5100-5107.

PEGylated FePt-Fe_3O_4 Composite Nanoassemblies (CNAs): *In vitro* Hyperthermia, Drug Delivery and generation of Reactive Oxygen Species (ROS)

Niroj Kumar Sahu,[1,2] Jagriti Gupta[1] and Dhirendra Bahadur[1*]

[1]*Department of Metallurgical Engineering and Materials Science, Indian Institute of Technology Bombay, Mumbai-400 076, India*

[2]*Centre for Nanotechnology Research, Vellore Institute of Technology University, Tamil Nadu-632014, India*

[*]Corresponding author: dhirenb@iitb.ac.in, Tel: +91-22-25767632, Fax: +91-22-2576 3480

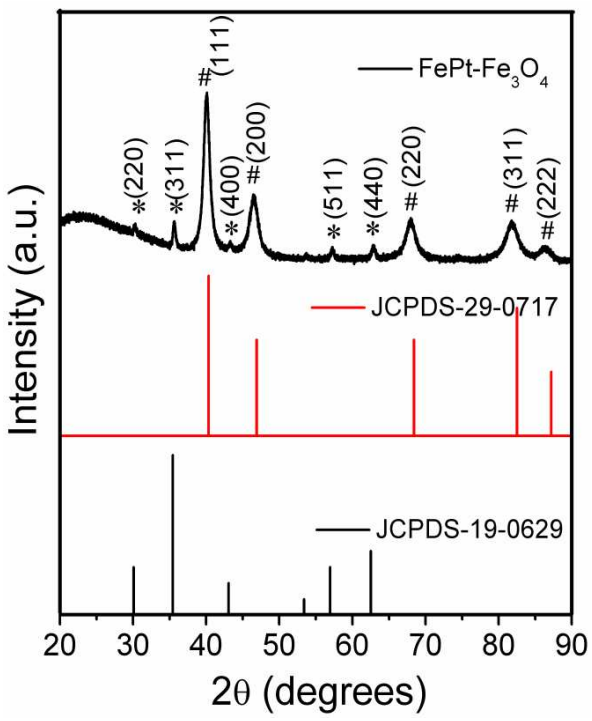

Fig. 1 XRD pattern of CNAs. The symbols # and * indicate the FePt and Fe_3O_4 phase, respectively.

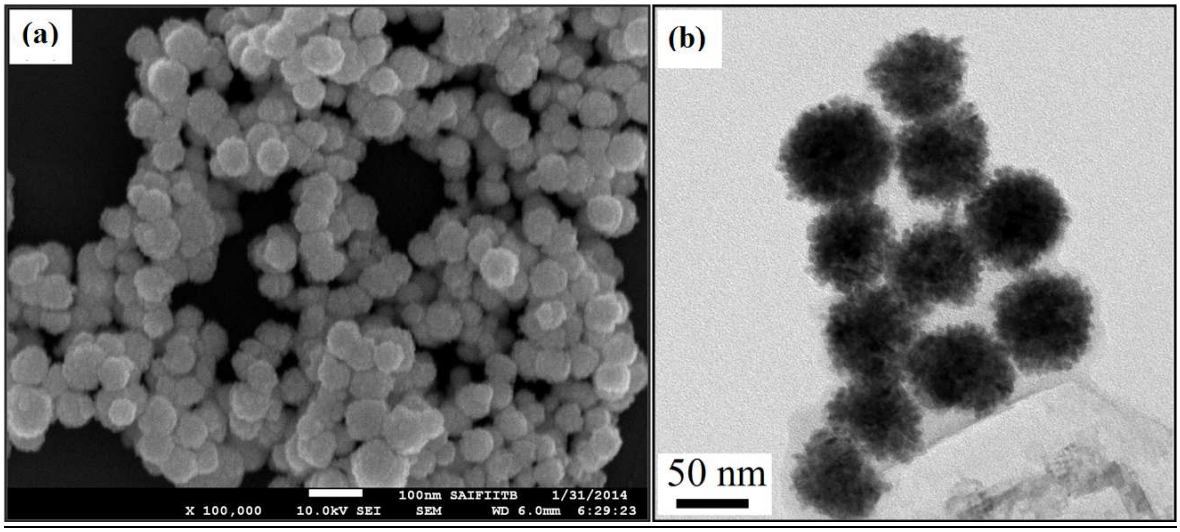

Fig. 2 (a) FESEM and (b) TEM images of the CNAs.

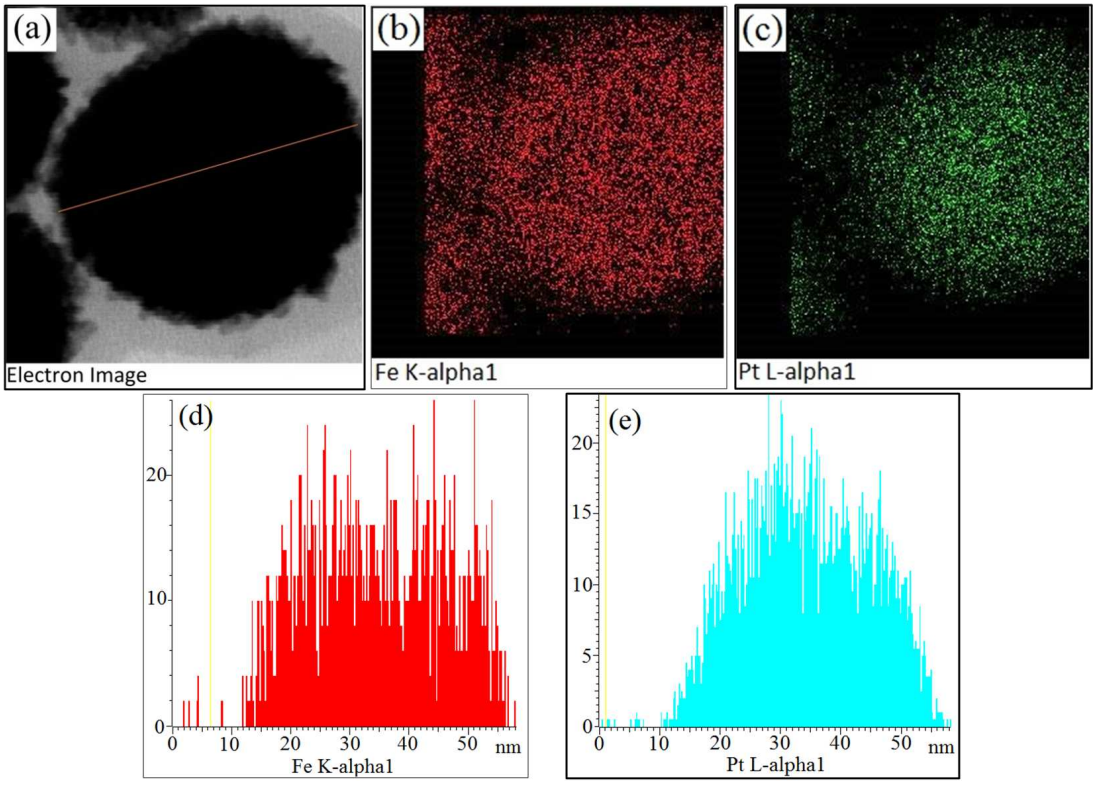

Fig. 3 (a) STEM image of the CNAs, Fig. (b and c) EDX spectra (area scanned) showing the variation of Fe and Pt and Fig. (d and e) line scanned images.

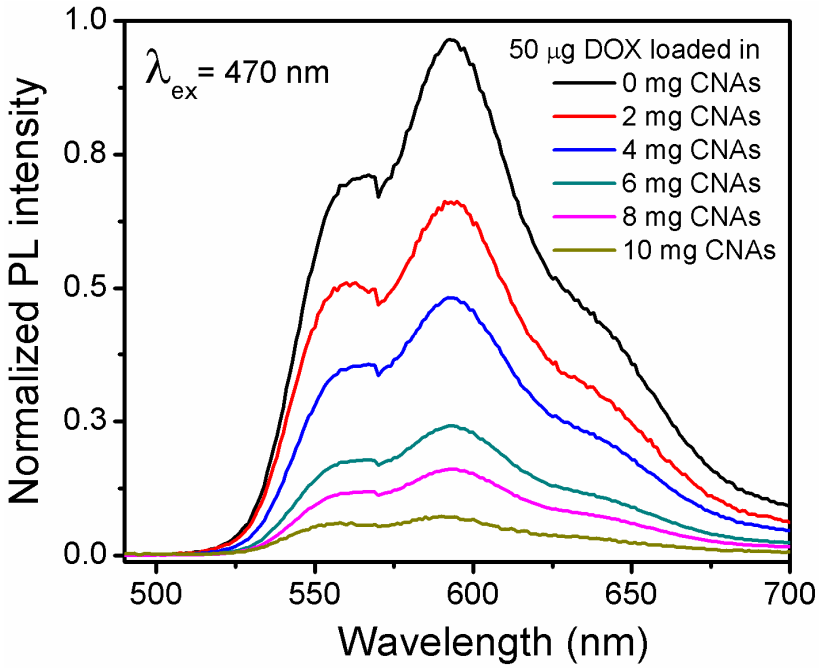

Fig. 4 Fluorescence spectra of the supernatant (unloaded part) after loading of 50 μg of DOX with different concentration of CNAs. The incubation time was kept fixed for 24 h. The excitation wavelength is 470 nm and the emission range is scanned between 490 and 700 nm.

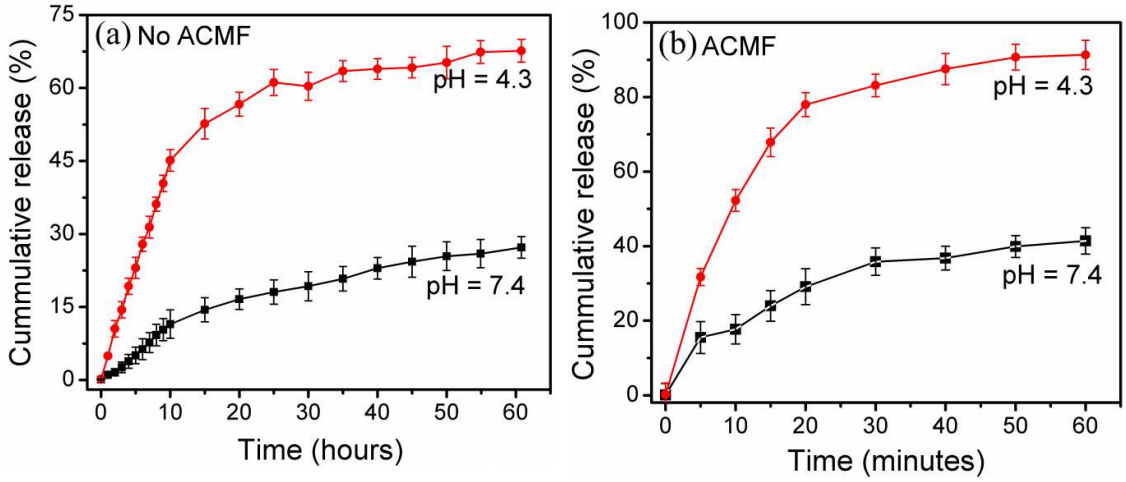

Fig. 5 Cumulative drug release profile from DOX loaded CNAs in cell mimicking environment at pH 7.4 and 4.3 without (a) and with (b) application of ACMF. PBS solution was taken as reservoir.

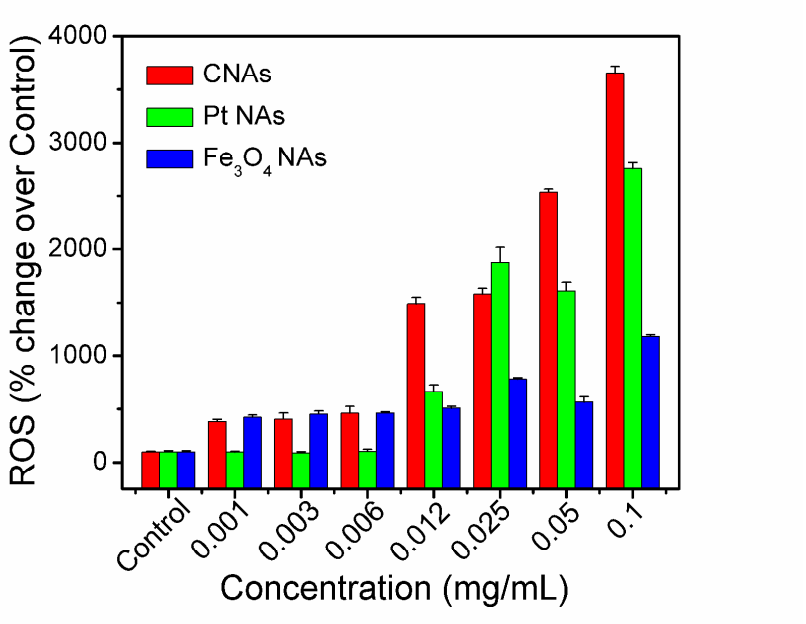

Fig. 6 Percentage change of ROS over control after treatment with different concentration of CNAs.

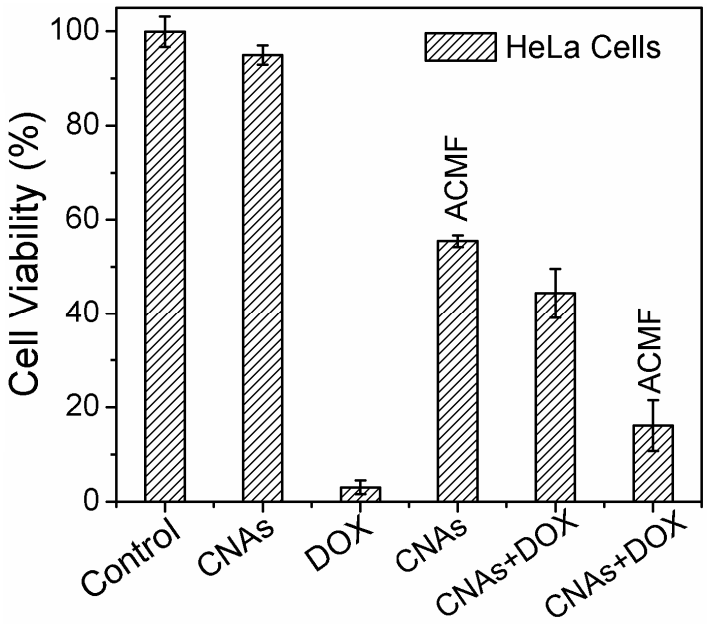

Fig. 7 *In vitro* cytotoxicity to HeLa cell lines with DOX, CNAs and CNAs + DOX with or without ACMF.

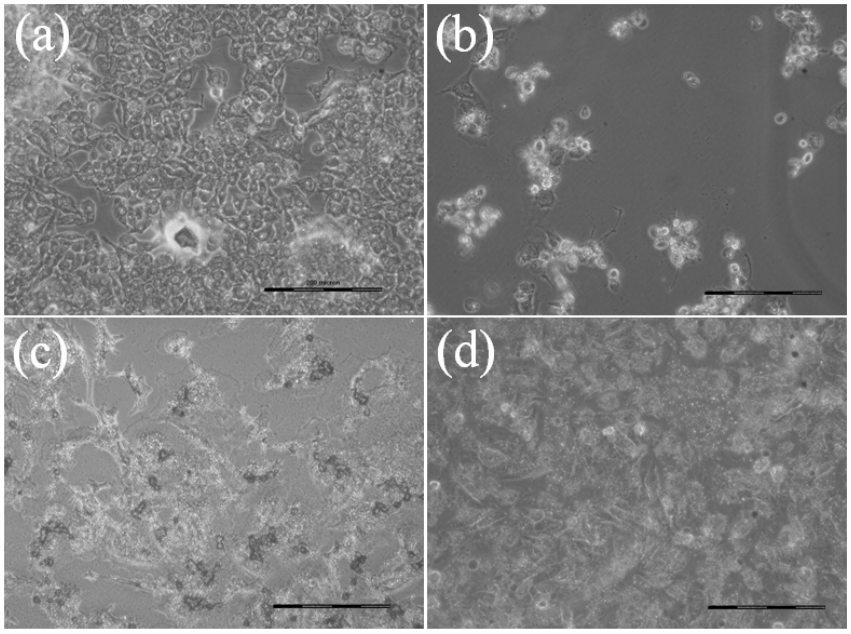

Fig. 8 Microscopic images of HeLa cells: (a) control, (b) after treatment with bare DOX, (c) after treatment with DOX loaded CNAs and (d) after treatment with DOX loaded CNAs in hyperthermia condition. All scale bars are 200 μm.

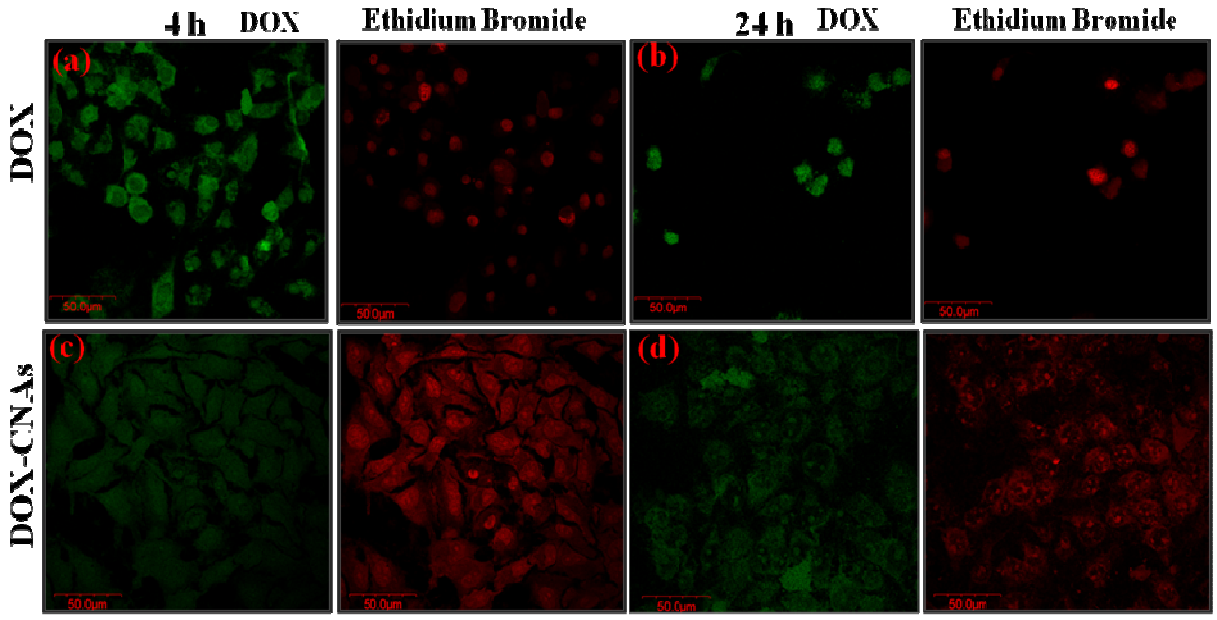

Fig. 9 Confocal laser scanning microscopy (CLSM) images show the apoptosis (DNA fragmentation) in HeLa cells: (a and b) with DOX (9 µg/mL) at indicated time intervals of 4 and 24 h, (c and d) with DOX loaded CNAs at indicated time intervals of 4 and 24 h. The green fluorescence shows the presence of DOX in DOX loaded CNAs, red fluorescence shows ethidium bromide (EtBr) stained nuclei. The scale bar is 50 µm

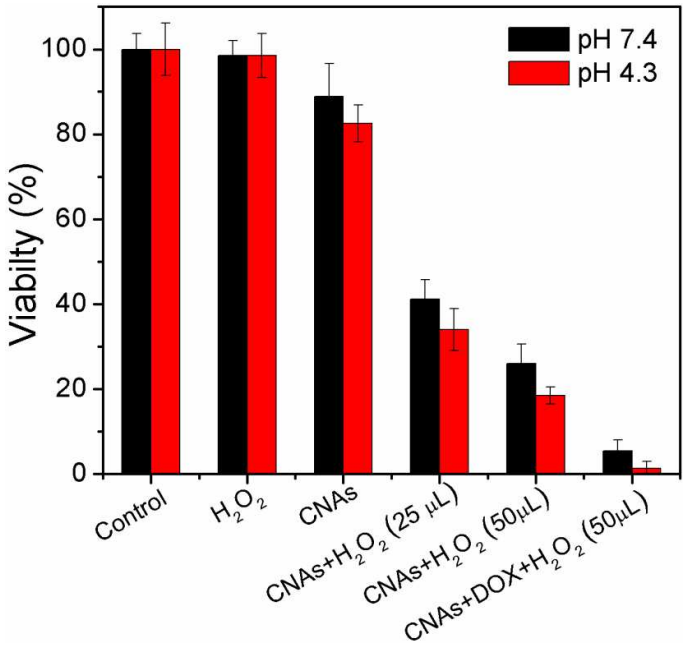

Fig. 10 *In vitro* cytotoxicity to HeLa cell lines with H_2O_2, CNAs+H_2O_2 and CNAs+DOX+H_2O_2 along with the control. The volume taken for H_2O_2 was 10 µL.